Lung CT Image Registration Using Diffeomorphic Transformation Models

Gang Song[1], Nicholas Tustison[1], Brian Avants[1], James C. Gee[1],

Penn Image Computing and Science Laboratory (PICSL), Dept. of of Radiology, University of Pennsylvania, Philadelphia, PA, USA,

Abstract. Given the importance of quantifying kinematics in the lung and segmenting its complex structure, various algorithms have been proposed in the literature for inter-subject and intra-subject lung registration. in this work, we describe the use of our ANTS open source software package in the EMPIRE10 challenge. Specifically, we describe the results of applying a subset of possible algorithmic configurations focusing on ANTS diffeomorphic transformation models: greedy Symmetric Normalization and exponential mappings. Both of which have been described in the literature and ultimately placed 1^{st} and 11^{th} respectively in the pre-conference portion of the EMPIRE10 challenge evaluating 34 total algorithms. The results show that our general image registration algorithm is able to achieve the state-of-the-art performance and is reproducible by using the same set of parameters in a fully automatic and open source pipeline.

1 Introduction

According to the American Lung Association, one in seven deaths in the United States is attributed to lung disease, and more than 35 million Americans live with chronic lung disease ([1]). Image techniques like multi-slice computed tomography provide a noninvasive way to study pulmonary morphology and function.

To accurately quantitfy both global and regional assessments of lung biomechanics from image data, automatic non-rigid image registration algorithm plays an important role. It computes a transformation mapping between two configurations of the lung at inspiration and expiration, from which measures of local deformation can be calculated and compared within and across subjects.

Various lung image registration algorithms have been proposed in the literature. A small sample includes optical flow ([2, 3]), compressed optical flow ([4]), Laplacian-filtered image ([5, 6]), free-form deformation ([7, 8]). In this paper we are interested in diffeomorphic transformations which, by definition, preserve topology. Topology preservation is fundamental to making comparisons between objects in the natural world as such transformations permit comparisons to be made across time points in an individual's disease process or to study development patterns across a large population. This fits naturally for the study of pulmonary kinematics. Some recent work on applying diffeomorphic transformation models on lung image registration includes [9, 10].

In this paper we apply two different diffeomorphic models to the data sets provided for the EMPIRE10 lung registration evaluation [11], using our open-source toolbox ANTS (Advanced Normalization Tools, [12]). Built on the ITK (Insight Segmentation and Registration Toolkit [13]) framework, this software package comprises a suite of tools for image normalization and template building based on previously published research. The results indicate that ANTS provides a competitive set of registration tools for intra-subject lung CT image registration.

2 Methods

A useful classification schema of image registration techniques is based upon the following three principal components ([14, 15]):

- the *transformation model*,
- the *similarity (or correspondence) measures*, and
- the *optimization strategy*.

In general, image registration is the process of finding the optimal transformation, ϕ, within a specified transformation space which maps each $\mathbf{x}$ of image $\mathcal{I}(\mathbf{x})$ to a location in image $\mathcal{J}(\mathbf{z})$ such that a specified cost function, $\mathcal{C}$, defined on $\mathcal{I}$, $\mathcal{J}$ and ϕ, is minimized.

One typical setting of lung CT image registration for pulmonary kinematics consists of two chest CT images at different phases of a breathing cycle of the same subject (i.e. the scenario in EMPIRE10 [11]). Following a commonly adopted two-step strategy, our registration pipeline begins with an affine transformation for initial global alignment, which precedes a deformable diffeomorphic transformation with increased degrees of freedom.

2.1 Affine Transformation

The affine transformation is optimized with respect to translation, rotation, scaling and shearing. The successive optimization of each component allows for individual control over increasing degrees of freedom.

The given lung masks of each image pair were the input to the affine registration. For these binary masks, mutual information([16, 17]) was used as the similarity function. More implementation details about the affine registration can be found in [18].

2.2 Diffeomorphic Transformations

In contrast to many other transformation models which reside in the domain of vector spaces, a diffeomorphism is a differentiable mapping with a differentiable inverse. Modeling transformations with diffeomorphisms ensures certain unique and desirable topological properties.

We assume that the diffeomorphism, ϕ, is defined on the image domain, Ω, and maintains an affine transform at the boundary such that $\phi(\partial\Omega) = A(\mathbf{Id})$ where $A(\mathbf{Id})$ is an affine mapping applied to the identity transformation. ϕ, over time, parameterizes a family of diffeomorphisms, $\phi(\mathbf{x}, t) : \Omega \times t \rightarrow \Omega$, which can be generated by integrating a time-dependent, smooth velocity field, $\boldsymbol{v} : \Omega \times t \rightarrow \mathbb{R}^d$, through the ordinary differential equation (o.d.e.)

$$\frac{d\phi(\mathbf{x}, t)}{dt} = \boldsymbol{v}(\phi(\mathbf{x}, t), t), \;\; \phi(\mathbf{x}, 0) = \mathbf{x}. \tag{1}$$

The deformation field yielded by ϕ is $\mathbf{u}(\mathbf{x}) = \phi(\mathbf{x}, 1) - \mathbf{x}$.

The following minimizing variational form was proposed for optimization in diffeomorphic normalization for inexact image matching in [19–21]:

$$\boldsymbol{v}^* = \underset{\boldsymbol{v}}{\operatorname{argmin}} \left\{ \int_0^1 ||L\boldsymbol{v}||^2 dt + \lambda \int_\Omega ||\mathcal{I} \circ \phi(\mathbf{x}, 1) - \mathcal{J}||^2 d\Omega \right\}. \tag{2}$$

The first term on the right represents a mathematical metric between $\mathcal{I}$ and $\mathcal{J}$ given an appropriate norm, L, on the velocity field, $\boldsymbol{v}$. The second term is the image similarity metric of square intensity difference with weight λ accounting for the inexact matching. To accommodate a variety of medical image normalization tasks, one typically encounters more complex intensity transfers between one anatomical instance $\mathcal{J}$ and another instance $\mathcal{I}$. This leads to the generalization of Equation (2):

$$\boldsymbol{v}^* = \underset{\boldsymbol{v}}{\operatorname{argmin}} \left\{ \int_0^1 ||L\boldsymbol{v}||^2 dt + \lambda \int_\Omega \mathit{\Pi}_\sim(\mathcal{I}, \phi(\mathbf{x}, 1), \mathcal{J}) d\Omega \right\} \tag{3}$$

where $\mathit{\Pi}_\sim$ is a similarity metric depending on the images and the mapping and λ controls the degree of exactness in the matching.

Symmetric Normalization Exploiting the fact that the diffeomorphism, ϕ, can be decomposed into two components ϕ_1 and ϕ_2, [22] constructs a *symmetric* alternative to Equation (3). This leads to the symmetric variant of Equation (3)

$$\begin{aligned} \{\boldsymbol{v}_1^*, \boldsymbol{v}_2^*\} = \underset{\boldsymbol{v_1}, \boldsymbol{v_2}}{\operatorname{argmin}} \Bigg\{ & \int_0^{0.5} \left(||L\boldsymbol{v}_1(x, t)||^2 + ||L\boldsymbol{v}_2(x, t)||^2 \right) dt \\ & + \lambda \int_\Omega \mathit{\Pi}_\sim \left(\mathcal{I} \circ \phi_1(\mathbf{x}, 0.5), \mathcal{J} \circ \phi_2(\mathbf{x}, 0.5) \right) d\Omega \Bigg\}. \end{aligned} \tag{4}$$

The corresponding symmetric Euler-Lagrange equations are similar to [20]. Finding $\boldsymbol{v_1}^*$ minimizes the variational energy from $t = 0$ whereas $\boldsymbol{v_2}^*$ minimizes from $t = 1$. Thus, gradient-based iterative convergence deforms $\mathcal{I}$ and $\mathcal{J}$ along the geodesic diffeomorphism, ϕ, to a fixed point midway between $\mathcal{I}$ and $\mathcal{J}$ thus motivating the denotation of the solution strategy as Symmetric Normalization (SyN).

In practice to reduce the significant computational and memory cost of the dense-in-time gradient calculations and requisite reintegration of the diffeomorphisms after each iterative update, we offer a greedy variant as a lower-cost alternative:

$$\nabla \Pi = \frac{\partial}{\partial \phi_i} \Pi_{\sim}(\mathcal{I}(\phi_1^{-1}(\mathbf{x}, 0.5)), \mathcal{J}(\phi_2^{-1}(\mathbf{x}, 0.5))) \tag{5}$$

for $i \in \{1, 2\}$. $\phi_1(\mathbf{x}, 0.5)$ and $\phi_2(\mathbf{x}, 0.5)$ are then updated from the previous iteration according to

$$\phi_i(\mathbf{x}, 0.5) = \phi_i(\mathbf{x}, 0.5) + \delta(K \star \nabla \Pi(\phi_i(\mathbf{x}, 0.5))). \tag{6}$$

where δ is a user-specified step parameter. K is the Green kernel of L, which is approximated by a Gaussian kernel ([23]). The gradient is then mapped back to the origin of each diffeomorphism to update the full mapping by enforcing $\phi^{-1}(\phi(\mathbf{x}, 1)) = \mathbf{x}$.

Exponential Mapping Ashburner introduced DARTEL (Diffeomorphic Anatomical Registration using Exponentiated Lie algebra) as a rapidly computed alternative to time parameterized diffeomorphic schemes ([24]). The key difference between a time-varying diffeomorphism and a diffeomorphism generated by an exponential mapping ([24]) is that the exponential mapping maintains only a single vector field that is constant in time.

By exponentiation of a constant velocity field, a diffeomorphism can be generated from the following o.d.e (cf Equation (1))

$$\frac{d\phi(\mathbf{x}, t)}{dt} = \boldsymbol{v}(\phi(\mathbf{x}, t)), \;\; \phi(\mathbf{x}, 0) = \mathbf{x}. \tag{7}$$

Note that there is no explicit time parameter in the velocity field. Theoretically, restricting the velocity field to be constant in time reduces the size of the space that may be generated ([25]).

2.3 Cross Correlation Similarity Metric

Previous research uses optical flow ([2, 3]) or its variant ([4]), which implicitly assumes the intensity consistency between two image. However, for the lung imaging, the image pair are usually from two breathing phases, in which the local density changes are linearly reflected in the intensity changes. In this case, the invariance of cross correlation to the linear intensity change makes it a suitable similarity function. Furthermore we compute cross correlation in a neighborhood around each voxel to accommodate the inhomogeneity of the density changes throughout the whole lung. The local cross correlation is integrated over the lung volume as the overall similarity in the diffeomorphic transformation. One may write the (squared) cross-correlation for the diffeomorphic image registration as:

$$\Pi_{\sim}(\mathcal{I}, \mathcal{J}) = \mathrm{CC}(\mathbf{x}) = \frac{(\sum_i (\mathcal{I}(\mathbf{x}_i) - \mu_{I(\mathbf{x})})(\mathcal{J}(\mathbf{x}_i) - \mu_{J(\mathbf{x})}))^2}{\sum_i (\mathcal{I}(\mathbf{x}_i) - \mu_{I(\mathbf{x})})^2 \sum_i (\mathcal{J}(\mathbf{x}_i) - \mu_{J(\mathbf{x})})^2}, \tag{8}$$

where $\mathbf{x}$ is at the center of N^3 square window, μ is the mean value within the window centered at $\mathbf{x}$ and $\mathbf{x}_i$ iterates through that window.

2.4 Optimization Strategy

The affine registration of the binary lung masks was used to initialize the transform. We composed the affine transformation with the deformable transformation field before performing any interpolation or downsampling. In this way, the image warping never required more than a single image interpolation step and was able to always refer back to the original full-resolution image sources.

The greedy Symmetric Normalization and the exponential mapping were then used separately for the following diffeomorphic deformable registrations. Both the affine and the two diffeomorphic image registrations were computed using our open source toolbox ANTS ([12]). For the diffeomorphic registration, the intensity values outside the lung masks were set to zeroes. The intensity values inside the lung masks were normalized to the range of $[0, 1]$ by the linear adjustment: $\frac{\max(I) - I}{\max(I) - \min(I)}$.

For both the affine and diffeomorphic registration, the gradient descent was used in the optimization. Convergence during the optimization is achieved if the slope of linear regression of the cost values of last 12 iterations is close to zero. A multi-resolution approach was applied in both steps to accelerate computation speed and avoid trapped in local minimum.

3 Results

The dataset of 20 pairs of chest CT scans was provided in the EMPIRE10 competition ([11]), as part of MICCAI 2010 Grand Challenges. Each pair of scans is taken from a single subject, in other words no inter-subject registrations are included. The scans come from a variety of sources and are provided by several different institutions. Scans may be taken at various phases in the breathing cycle (full inspiration, full expiration, phase from 4D breathing data). Subjects may exhibit lung disease or appear healthy. Data from a variety of scanners are included and a variety of voxel sizes occur. In addition to the CT data, binary lung masks are provided for each scan. The lung masks are automatically generated using an algorithm by van Rikxoort et al. [26]. They have been visually checked and manually corrected where necessary.

We reported results of two methods in this paper. Both used the same affine registration on the lung masks to initialize the deformation. In the step of diffeomorphic registration, the first method used greedy SyN (noted as *gsyn*) and the second used exponential mapping (noted as *exp*). The registration process was fully automatic. The same set of parameters was used across all image pairs. The affine registration applied a four-level image pyramid and 10^4 locations were sampled in computing the mutual information of the lung binary masks. A five-level image pyramid was applied in both *gsyn* and *exp*. The neighborhood radius

	Lung Boundaries		Fissures		Landmarks		Singularities		
Scan Pair	**Score**	**Rank**	**Score**	**Rank**	**Score**	**Rank**	**Score**	**Rank**	**Time**
01	0.00	6.00	0.00	1.00	1.18	2.00	0.00	11.50	6h 28m
02	0.00	11.00	0.00	15.00	0.34	3.00	0.00	12.50	8h 13m
03	0.00	5.50	0.00	12.50	0.29	1.00	0.00	12.00	7h 1m
04	0.00	2.50	0.00	16.50	0.84	4.00	0.00	14.00	7h 52m
05	0.00	13.00	0.00	16.00	0.00	5.50	0.00	13.50	3h 44m
06	0.00	16.00	0.00	15.00	0.30	7.00	0.00	14.00	2h 40m
07	0.00	1.50	0.08	2.00	1.14	1.00	0.00	10.00	7h 47m
08	0.00	4.00	0.00	3.50	0.59	3.00	0.00	12.50	7h 40m
09	0.00	2.00	0.00	6.50	0.50	2.00	0.00	13.00	7h 7m
10	0.00	1.50	0.00	15.00	1.55	12.00	0.00	13.50	8h 26m
11	0.01	13.00	0.00	4.00	0.65	4.00	0.00	11.50	6h 1m
12	0.00	10.00	0.00	13.50	0.00	1.50	0.00	14.50	6h 32m
13	0.00	3.00	0.07	7.00	0.76	3.00	0.00	13.00	2h 6m
14	0.00	2.00	0.21	2.00	0.80	1.00	0.00	9.50	8h 11m
15	0.00	8.00	0.00	7.00	0.58	1.00	0.00	12.50	5h 9m
16	0.00	3.50	0.01	10.00	0.93	5.00	0.00	13.50	55m
17	0.00	6.50	0.07	30.00	0.64	3.00	0.00	14.00	1h 22m
18	0.00	1.00	0.00	1.00	0.94	1.00	0.00	21.00	12h41m
19	0.00	14.00	0.00	12.00	0.45	3.00	0.00	14.50	7h 9m
20	0.00	3.50	0.14	1.00	0.83	1.00	0.00	10.50	7h 42m
Avg	0.00	6.37	0.03	9.52	0.66	3.20	0.00	13.05	
Average Ranking Overall								8.03	
Final Placement								1	

Table 1. Results using greedy SyN for each scan pair, per category and overall. Rankings and final placement are from a total of 34 competing algorithms. The total running time for each pair is shown on the last column.

in computing cross correlation was 2 voxels. The Gaussian regularization kernel width was 6 voxels.

The deformation fields were evaluated in four categories: lung boundaries, fissure alignments, labeled landmarks and singularities in the deformation. More details about the evaluation and ranking protocol can be found in [11]. Table 1 shows the evaluation results of our greedy Symmetric Normalization model *gsyn*. Table 2 shows the corresponding results for the exponential mapping model. Computation was performed on a Linux workstation of Intel Xeon QuadCore CPU at 3GHz with 16 GB main memory.

Out of the 34 submitted algorithms, our *gsyn* got the first placement in the overall ranking and *exp* got the 11th. Greedy SyN outperformed exponen-

	Lung Boundaries		Fissures		Landmarks		Singularities		
Scan Pair	**Score**	**Rank**	**Score**	**Rank**	**Score**	**Rank**	**Score**	**Rank**	**Time**
01	0.00	2.50	0.21	14.00	2.46	13.00	0.01	27.00	8h 27m
02	0.00	11.00	0.00	15.00	0.44	13.00	0.00	12.50	10h 3m
03	0.00	5.50	0.00	12.50	0.41	14.00	0.00	12.00	8h 23m
04	0.00	2.50	0.00	16.50	1.59	20.00	0.00	28.00	10h11m
05	0.00	13.00	0.00	16.00	0.00	5.50	0.00	13.50	6h 54m
06	0.00	16.00	0.00	2.00	0.37	16.00	0.00	14.00	4h 7m
07	0.00	6.00	1.44	18.00	2.82	15.00	0.00	25.00	8h 53m
08	0.00	4.00	0.04	15.00	1.16	17.00	0.00	26.00	8h 31m
09	0.00	6.00	0.00	20.00	0.59	14.00	0.00	13.00	8h 5m
10	0.00	1.50	0.00	15.00	3.00	20.00	0.03	28.00	9h 16m
11	0.04	16.00	0.09	16.00	1.15	13.00	0.00	25.00	8h 14m
12	0.00	10.00	0.02	28.00	0.27	20.00	0.00	14.50	5h 14m
13	0.00	3.00	0.06	2.50	1.08	18.00	0.00	13.00	2h 41m
14	0.00	3.00	5.78	20.00	2.35	10.00	0.01	26.00	9h 13m
15	0.00	8.00	0.00	7.00	0.64	13.00	0.00	12.50	7h 56m
16	0.00	3.50	0.01	8.50	1.38	20.00	0.00	13.50	1h 8m
17	0.00	6.50	0.05	16.00	0.98	16.00	0.00	14.00	2h 2m
18	0.00	4.00	0.90	9.00	2.93	16.00	0.00	24.00	7h 45m
19	0.00	14.00	0.00	26.00	0.50	13.00	0.00	29.00	9h 32m
20	0.00	3.50	1.99	10.00	1.70	10.00	0.00	25.00	8h 52m
Avg	0.00	6.97	0.53	14.35	1.29	14.82	0.00	19.77	
Average Ranking Overall								13.98	
Final Placement								11	

Table 2. Results using exponential mapping for each scan pair, per category and overall. Rankings and final placement are from a total of 34 competing algorithms. The total running time for each pair is shown on the last column.

tial mapping, which shows the benefit using time-dependent velocity field over constant-in-time velocity field in this application. In general, greedy SyN gave a satisfactory registration result. Most fissures and lung boundaries were aligned well with error close to zero. There are almost no singularities in the deformation fields due to the theoretical properties of diffeomorphic transformation models. [1] The average displacement of the manually labeled landmarks was within one

[1] Some Jacobian values of the deformation fields were reported as negative, which are contradictory to the definition of diffeomorphism. A closer examination at these values shows that they are on the image boundaries, where the numerical computation of Jacobian values may not be accurate.

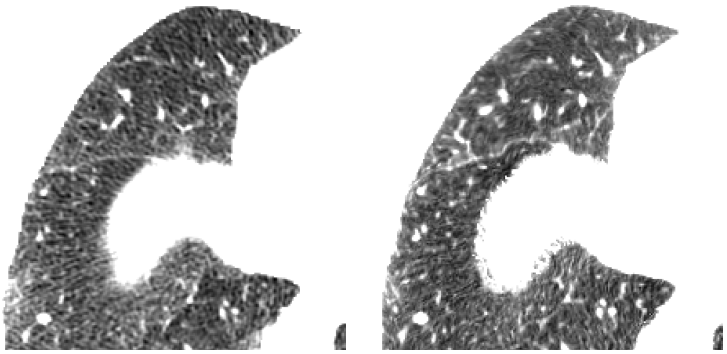

(a) Fixed image (b) Warped image

Fig. 1. Example of bad registration shown in enlarged image region. The vessels and the fissure in the upper region do not align well. The remaining lower region, however, has a good registration.

voxel for most pairs after registration. An example of bad result is illustrated in Fig.1, where the vessels in the upper half of the image were not aligned.

4 Discussion

In this paper we applied two diffeomorphic transformation models to the data provided by the EMPIRE10 challenge. Cross correlation was used as the similarity function to compensate the intensity change in the lung volumes at different breathing phases. By carefully choosing the parameters, e.g. the cross correlation window size and the Gaussian regularization kernel width, for the specific application, our general image registration algorithm is able to achieve a competitive result among other state-of-the-art methods, with the greedy Symmetric Normalization ranked No.1 and the exponential mapping ranked No.11 in the final outcome involving a total of 34 algorithms.

The whole registration pipeline was built on ANTS, an open-source toolbox and publicly available. We should note that as a general purpose image registration software, ANTS has demonstrated success in other applications [27, 28]. Besides the image preprocessing, the programming of registration pipeline involved simple scripting, which makes the results reproducible. We believe that such an open source toolbox could benefit the research community and promote the idea of *reproducible research*, as described by Dr. Kovacevic ([29]), which "refers to the idea that, in "'computational' sciences, the ultimate product is not a published paper but, rather, the entire environment used to produce the results in the paper (data, software,etc.)."

There are still places to improve in the accuracy of current registration results. As shown in Fig.1, some blood vessels and fissures were not aligned. More domain specific knowledge, like the positions of the vessels and fissures from

lung anatomy segmentation, should be utilized to improve upon current general registration techniques. The running time cost for our diffeomorphic approaches is very high (see last column in Table 1 and 2). The running time is linear to the volume size multiplied by the number of iterations. This can be improved by exploring possibilities of multi-threading computation and GPU technology in the future implementation.

References

1. American Lung Association: Lung disease data: 2006 (2006)
2. Guerrero, T., Castillo, R., Noyola-Martinez, J., Torres, M., Zhou, X., Guerra, R., Cody, D., Komaki, R., Travis, E.: Reduction of pulmonary compliance found with high-resolution computed tomography in irradiated mice. Int J Radiat Oncol Biol Phys **67**(3) (Mar 2007) 879–887
3. Dawood, M., Buther, F., Jiang, X., Schafers, K.P.: Respiratory motion correction in 3-d pet data with advanced optical flow algorithms. IEEE Trans Med Imaging **27**(8) (Aug 2008) 1164–1175
4. Castillo, E., Castillo, R., Zhang, Y., Guerrero, T.: Compressible image registration for thoracic computed tomography images. Journal of Medical and Biological Engineering **29**(5) (2009) 222–233
5. Dougherty, L., Asmuth, J.C., Gefter, W.B.: Alignment of ct lung volumes with an optical flow method. Acad Radiol **10**(3) (Mar 2003) 249–254
6. Dougherty, L., Torigian, D.A., Affusso, J.D., Asmuth, J.C., Gefter, W.B.: Use of an optical flow method for the analysis of serial CT lung images. Acad Radiol **13**(1) (Jan 2006) 14–23
7. Sarrut, D., Delhay, B., Villard, P.F., Boldea, V., Beuve, M., Clarysse, P.: A comparison framework for breathing motion estimation methods from 4-d imaging. IEEE Trans Med Imaging **26**(12) (Dec 2007) 1636–1648
8. Wu, Z., Rietzel, E., Boldea, V., Sarrut, D., Sharp, G.C.: Evaluation of deformable registration of patient lung 4dct with subanatomical region segmentations. Medical Physics **35**(2) (2008) 775–781
9. Cook, T.S., Tustison, N., Biederer, J., Tetzlaff, R., Gee, J.: How do registration parameters affect quantitation of lung kinematics? Med Image Comput Comput Assist Interv Int Conf Med Image Comput Comput Assist Interv **10**(Pt 1) (2007) 817–824
10. Gee, J., Sundaram, T., Hasegawa, I., Uematsu, H., Hatabu, H.: Characterization of regional pulmonary mechanics from serial magnetic resonance imaging data. Acad Radiol **10**(10) (Oct 2003) 1147–1152
11. K. Murphy, B.v.G., Reinhardt, J., Kabus, S., Ding, K.: Evaluation of Methods for Pulmonary Image Registration: The EMPIRE10. (2010)
12. Avants, B.B., Tustison, N.J., Song, G., Gee, J.C.: ANTS, Advanced Normalization Tools. http://www.picsl.upenn.edu/ANTS/. (2010)
13. National Library of Medicine: ITK,Insight Segmentation and Registration Toolkit. http://www.itk.org
14. Brown, L.G.: A survey of image registration techniques. ACM Computing Surveys **24**(4) (December 1992) 325–376
15. Ibanez, L., Ng, L., Gee, J.C., Aylward, S.: Registration patterns: The generic framework for image registration of the Insight Toolkit. In: IEEE International Symposium on Biomedical Imaging. (July 2002) 345–348
16. Viola, P., Wells, W.M.: Alignment by maximization of mutual information. International Journal of Computer Vision **24**(2) (1997) 137–154

17. Maes, F., Collignon, A., Vandermeulen, D., Marchal, G., Suetens, P.: Multimodality image registration by maximization of mutual information. IEEE Trans Med Imaging **16**(2) (Apr 1997) 187–198
18. Song, G., Avants, B., Gee, J.: Multi-start method with prior learning for image registration. In: Proceedings of the Workshop on Mathematical Methods in Biomedical Image Analysis. (2007)
19. Dupuis, P., Grenander, U., Miller, M.I.: Variational problems on flows of diffeomorphisms for image matching. (1998)
20. Miller, M.I., Trouve, A., Younes, L.: On the metrics and euler-lagrange equations of computational anatomy. Annu Rev Biomed Eng **4** (2002) 375–405
21. Beg, M.F., Miller, M.I., Trouvé, A., Younes, L.: Computing large deformation metric mappings via geodesic flows of diffeomorphisms. Int. J. Comput. Vision **61**(2) (2005) 139–157
22. Avants, B., Anderson, C., Grossman, M., Gee, J.C.: Spatiotemporal normalization for longitudinal analysis of gray matter atrophy in frontotemporal dementia. Med Image Comput Comput Assist Interv Int Conf Med Image Comput Comput Assist Interv **10**(Pt 2) (2007) 303–310
23. Bro-Nielsen, M., Gramkow, C.: Fast fluid registration of medical images. In: VBC '96: Proceedings of the 4th International Conference on Visualization in Biomedical Computing, London, UK, Springer-Verlag (1996) 267–276
24. Ashburner, J.: A fast diffeomorphic image registration algorithm. Neuroimage **38**(1) (Oct 2007) 95–113
25. Arnold, V.I.: Ordinary Differential Equations. Springer-Verlag (1991)
26. van Rikxoort, E.M., de Hoop, B., Viergever, M.A., Prokop, M., van Ginneken, B.: Automatic lung segmentation from thoracic computed tomography scans using a hybrid approach with error detection. Med Phys **36**(7) (Jul 2009) 2934–2947
27. Avants, B.B., Epstein, C.L., Grossman, M., Gee, J.C.: Symmetric diffeomorphic image registration with cross-correlation: evaluating automated labeling of elderly and neurodegenerative brain. Med Image Anal **12**(1) (Feb 2008) 26–41
28. Klein, A., Andersson, J., Ardekani, B.A., Ashburner, J., Avants, B., Chiang, M.C., Christensen, G.E., Collins, L.D., Gee, J., Hellier, P., Song, J.H., Jenkinson, M., Lepage, C., Rueckert, D., Thompson, P., Vercauteren, T., Woods, R.P., Mann, J.J., Parsey, R.V.: Evaluation of 14 nonlinear deformation algorithms applied to human brain mri registration. Neuroimage (Jan 2009)
29. Kovacevic, J.: From the editor-in-chief. IEEE Trans Image Proc **15**(12) (Dec 2006) 3625–3626